J Braz. Soc. Mech. Sci. Eng. (2015) 37:1623–1633
DOI 10.1007/s40430-014-0242-z

TECHNICAL PAPER

Effect of uniform suction on nanofluid flow and heat transfer over a cylinder

M. Sheikholeslami

Received: 9 May 2014 / Accepted: 19 August 2014 / Published online: 27 September 2014

Abstract The aim of the present paper is to study the nanofluid flow and heat transfer over a stretching porous cylinder. The effective thermal conductivity and viscosity of the nanofluid are calculated by KKL (Koo–Kleinstreuer–Li) correlation. In KKL model, the effect of Brownian motion on the effective thermal conductivity is considered. The governing partial differential equations with the corresponding boundary conditions are reduced to a set of ordinary differential equations with the appropriate boundary conditions using similarity transformation, which is then solved numerically by the fourth-order Runge–Kutta integration scheme featuring a shooting technique. Numerical results for flow and heat transfer characteristics are obtained for various values of the nanoparticle volume fraction, suction parameter, Reynolds number and different kinds of nanofluids. Results show that inclusion of a nanoparticle into the base fluid of this problem is capable to change the flow pattern. It is found that Nusselt number is an increasing function of nanoparticle volume fraction, suction parameter and Reynolds number.

Keywords Nanofluid · Boundary layer · Stretching cylinder · Heat transfer · Nonlinear ordinary differential equations

Technical Editor: Francisco Ricardo Cunha.

M. Sheikholeslami (✉)
Department of Mechanical Engineering, Babol University of Technology, Babol, Islamic Republic of Iran
e-mail: m.sheikholeslami@stu.nit.ac.ir

List of symbols

a	Radius of cylinder
c	Positive constant
C_f	Skin friction coefficient
f	Dimensionless stream function
k	Thermal conductivity
Nu	Nusselt number
P	Pressure
Pr	Prandtl number
q_w	Surface heat flux
Re	Reynolds number
T	Fluid temperature
T_w	Temperature of the cylinder surface
T_∞	Ambient temperature
(u, w)	Velocity components in the) r, z) directions, respectively
(r, z)	Cylindrical coordinates in the radial and axial directions, respectively
w_w	Velocity of the stretching cylinder

Greek symbols

α	Thermal diffusivity
η	Similarity variable
θ	Dimensionless temperature
μ	Dynamic viscosity
υ	Kinematic viscosity
ρ	Fluid density
τ_w	Surface shear stress
ψ	Stream function
γ	Suction parameter

Subscripts

w	Condition at the surface
∞	Condition at infinity
nf	Nanofluid

f Base fluid
s Nanosolid particles

1 Introduction

In recent decade, because of rising demands of modern technology, including chemical production, power station, and microelectronics, there is a need to develop new types of fluids that will be more effective in terms of heat exchange performance. Nanofluids are produced by dispersing the nanometer-scale solid particles into base liquids with low thermal conductivity such as water, ethylene glycol (EG) and oils. [1]. The term "nanofluid" was first coined by Choi [2] to describe this new class of fluids. The materials with sizes of nanometers possess unique physical and chemical properties [3]. Using nanofluid instead of base fluid increases the effective thermal conductivity of the fluid and consequently enhances the heat transfer characteristics. Sheikholeslami et al. [4] studied the magnetic field effect on CuO–water nanofluid flow and heat transfer in an enclosure which is heated from below. They found that effect of Hartmann number and heat source length is more pronounced at high Rayleigh number. Rashidi et al. [5] considered the analysis of the second law of thermodynamics applied to an electrically conducting incompressible nanofluid fluid flowing over a porous rotating disk. They concluded that magnetic rotating disk drives have important applications in heat transfer enhancement in renewable energy systems. Sheikholeslami et al. [6] studied the problem of MHD free convection in an eccentric semi-annulus filled with nanofluid. They showed that Nusselt number decreases with increase of position of inner cylinder at high Rayleigh number. Hatami et al. [7] investigated the magnetohydrodynamic Jeffery–Hamel nanofluid flow in non-parallel walls. They found that skin friction coefficient is an increasing function of Reynolds number, opening angle and nanoparticle volume friction but decrease function of Hartmann number. Therefore, numerous methods have been taken to improve the thermal conductivity of these fluids by suspending nano/micro-sized particle materials in liquids. Several numerical studies have been published recently on the modeling of natural convection heat transfer in nanofluids such as [8–39].

Steady flow in a viscous and incompressible fluid outside of a stretching hollow cylinder in an ambient fluid at rest has been performed by Wang [40]. The problem is governed by a third-order nonlinear ordinary differential equation that leads to exact similarity solutions of the Navier–Stokes equations. The flow over a cylinder can be considered as two-dimensional flow if the body radius is large compared to the boundary layer thickness. On the other hand for a thin or slender cylinder, the radius of the cylinder may be of the same order as that of the boundary layer thickness. The study of convective heat transfer in fluid-saturated porous media has many important applications in technology of geothermal energy recovery such as oil recovery, food processing, fiber and granular insulation, porous burner and heater, combustion of low-calorific fuels to diesel engines and design of packed bed reactors. In general, suction tends to increase the skin friction and heat transfer coefficients, whereas injection acts in the opposite manner [41]. The effects of suction/injection on the flow and heat transfer over a slender cylinder have attracted many researchers to make further investigations. The effect of slot suction/injection over a thin cylinder was studied by Datta et al. [42] and Kumari and Nath [43]. These papers may be useful in the cooling of nuclear reactors during emergency shutdown, where a part of the surface can be cooled by injecting a coolant. Ishak et al. [44] studied uniform suction/blowing effect on flow and heat transfer due to a stretching cylinder which is useful as a simple model in understanding more complicated applications to practical problems, such as cooling of nuclear reactors.

The objective of the present paper is to study the nanofluid flow and heat transfer due to a stretching cylinder with uniform suction. The effective thermal conductivity and viscosity of the nanofluid are calculated by KKL (Koo–Kleinstreuer–Li) correlation. In this model, the effect of Brownian motion on the effective thermal conductivity is considered. The reduced ordinary differential equations are solved numerically using the fourth-order Runge–Kutta integration scheme featuring a shooting technique. The effects of the parameters governing the problem are studied and discussed.

2 Problem formulation and equations

Consider the steady laminar nanofluid flow caused by a stretching tube with radius a in the axial direction in a fluid (Fig. 1), where the z-axis is measured along the axis of the tube and the r-axis is measured in the radial direction. It is assumed that the surface of the tube has constant temperature T_w and the ambient fluid temperature is T_∞ ($T_w > T_\infty$). The viscous dissipation is neglected as it is assumed to be small. It is assumed that the base fluid and the nanoparticles are in thermal equilibrium and no slip occurs between them. Under these assumptions the governing equations are:

Vector form:

$$\vec{\nabla} \cdot \vec{V} = 0 \tag{1}$$

$$\rho_{nf}\left(\frac{\partial \vec{V}}{\partial t} + \left(\vec{V} \cdot \vec{\nabla}\right)\vec{V}\right) = -\vec{\nabla} P + \mu_{nf}\nabla^2 \vec{V} \tag{2}$$

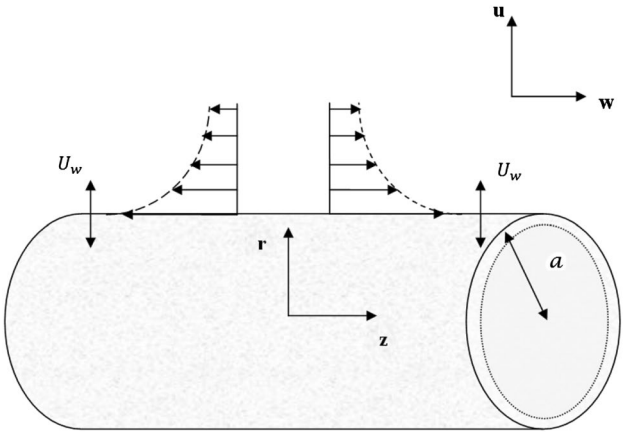

Fig. 1 Geometry of the problem

$$(\rho C_{\mathrm{p}})_{\mathrm{nf}}\left(\frac{\partial T}{\partial t}+\left(\vec{V}.\vec{\nabla}\right)T\right)=k_{\mathrm{nf}}\nabla^2 T \tag{3}$$

where $\vec{V}=(u,v,w)$ is velocity vector, $T$is temperature, $P$is pressure, $\rho_{\mathrm{nf}},\mu_{\mathrm{nf}},(C_{\mathrm{p}})_{\mathrm{nf}},k_{\mathrm{nf}}$ are density, viscosity, heat capacitance, thermal conductivity of nanofluid. Also the operation of $\vec{\nabla}$ can be defined as$\vec{\nabla}=\left(\frac{\partial}{\partial x},\frac{\partial}{\partial y},\frac{\partial}{\partial z}\right)$.

Scalar form:

$$\frac{\partial(rw)}{\partial z}+\frac{\partial(ru)}{\partial r}=0, \tag{4}$$

$$\rho_{\mathrm{nf}}\left(w\frac{\partial w}{\partial z}+u\frac{\partial w}{\partial r}\right)=\mu_{\mathrm{nf}}\left(\frac{\partial^2 w}{\partial r^2}+\frac{1}{r}\frac{\partial w}{\partial r}\right), \tag{5}$$

$$\rho_{\mathrm{nf}}\left(w\frac{\partial u}{\partial z}+u\frac{\partial u}{\partial r}\right)=-\frac{\partial P}{\partial r}+\mu_{\mathrm{nf}}\left(\frac{\partial^2 u}{\partial r^2}+\frac{1}{r}\frac{\partial u}{\partial r}-\frac{u}{r^2}\right) \tag{6}$$

$$\left(w\frac{\partial T}{\partial z}+u\frac{\partial T}{\partial r}\right)=\frac{k_{\mathrm{nf}}}{(\rho C_{\mathrm{p}})_{\mathrm{nf}}}\left(\frac{\partial^2 T}{\partial r^2}+\frac{1}{r}\frac{\partial T}{\partial r}\right), \tag{7}$$

subject to the boundary conditions

$$\begin{aligned} r=a \quad &: \quad u=U_{\mathrm{w}}, \quad w=w_{\mathrm{w}}\ , \quad T=T_{\mathrm{w}} \\ r\to\infty: \quad &w\to 0, \quad T\to T_{\infty} \end{aligned} \tag{8}$$

where $U_{\mathrm{w}}=-\mathrm{ca}\gamma, w_{\mathrm{w}}=2\mathrm{cz}$ and c is a positive constant. γ is a constant in which $\gamma>0$ and $\gamma<0$ corresponding to mass suction and mass injection, respectively.

The effective density(ρ_{nf}) and the heat capacitance $(\rho C_{\mathrm{p}})_{\mathrm{nf}}$ of the nanofluid are given as:

$$\rho_{\mathrm{nf}}=\rho_{\mathrm{f}}(1-\phi)+\rho_{\mathrm{s}}\phi \tag{9}$$

$$(\rho C_{\mathrm{p}})_{\mathrm{nf}}=(\rho C_{\mathrm{p}})_{\mathrm{f}}(1-\phi)+(\rho C_{\mathrm{p}})_{\mathrm{s}}\phi \tag{10}$$

Table 1 Thermo-physical properties of water and nanoparticles [45]

	ρ (kg/m^3)	C_{p} (j/kgk)	k (W/mk)	d_{p} (nm)	σ (Ω m)$^{-1}$
Pure water	997.1	4179	0.613	–	0.05
Al_2O_3	3970	765	25	47	10^{-12}
CuO	6500	540	18	29	10^{-10}

Table 2 The coefficient values of Al_2O_3–water nanofluids and CuO–water nanofluids [45]

Coefficient values	Al_2O_3–Water	CuO–Water
a_1	52.813488759	−26.593310846
a_2	6.115637295	−0.403818333
a_3	0.6955745084	−33.3516805
a_4	4.17455552786E−02	−1.915825591
a_5	0.176919300241	6.42185846658E−02
a_6	−298.19819084	48.40336955
a_7	−34.532716906	−9.787756683
a_8	−3.9225289283	190.245610009
a_9	−0.2354329626	10.9285386565
a_{10}	−0.999063481	−0.72009983664

Here, ϕ is the solid volume fraction.

The Brownian motion has a significant impact on the effective thermal conductivity. Koo and Kleinstreuer [45] proposed that the effective thermal conductivity is composed of the particle's conventional static part and a Brownian motion part. This 2-component thermal conductivity model takes into account the effects of particle size, particle volume fraction and temperature dependence as well as types of particle and base fluid combinations.

$$k_{\mathrm{eff}}=k_{\mathrm{static}}+k_{\mathrm{Brownian}} \tag{11}$$

$$\frac{k_{\mathrm{static}}}{k_{\mathrm{f}}}=1+\frac{3\left(\frac{k_{\mathrm{p}}}{k_{\mathrm{f}}}-1\right)\phi}{\left(\frac{k_{\mathrm{p}}}{k_{\mathrm{f}}}+2\right)-\left(\frac{k_{\mathrm{p}}}{k_{\mathrm{f}}}-1\right)\phi}, \tag{12}$$

where k_{static} is the static thermal conductivity based on Maxwell classical correlation. The enhanced thermal conductivity component generated by micro-scale convective heat transfer of a particle's Brownian motion and affected by ambient fluid motion is obtained via simulating Stokes' flow around a sphere (nanoparticle). By introducing two empirical functions (β and f) Koo [46] combined the interaction between nanoparticles in addition to the temperature effect in the model, leading to:

$$k_{\mathrm{Brownian}}=5\times 10^4\beta\phi\rho_{\mathrm{f}}c_{\mathrm{p,f}}\sqrt{\frac{\kappa_{\mathrm{b}}T}{\rho_{\mathrm{p}}d_{\mathrm{p}}}}f(T,\phi). \tag{13}$$

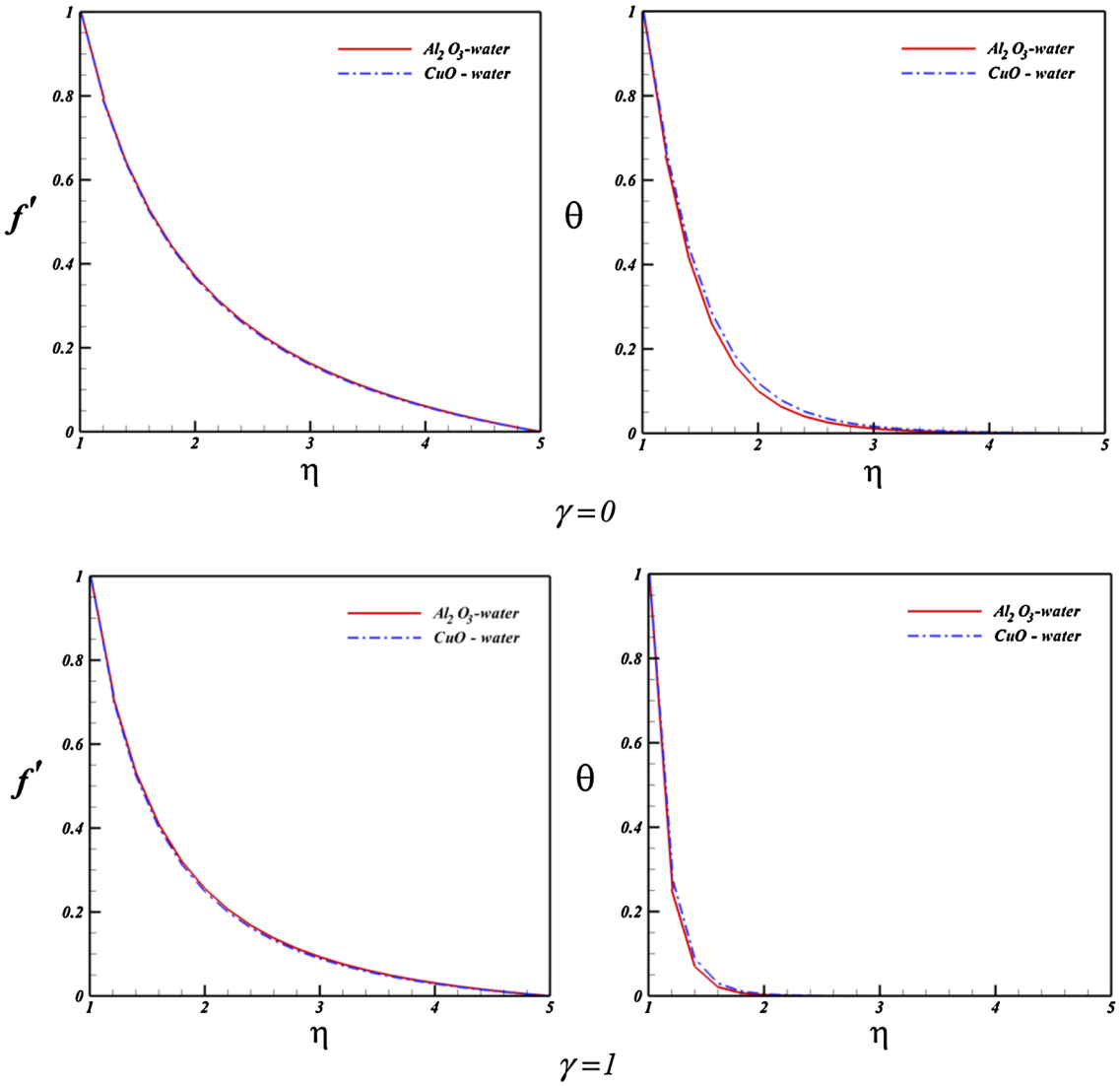

Fig. 2 Velocity profile and temperature distribution for different types of nanofluids when $\phi = 0.04$, Re = 1 and Pr = 6.8

Table 3 Effects of different kind of nanoparticles on skin friction coefficient when $\phi = 0.04$

γ	Re	Nanoparticles	
		CuO	Al_2O_3
0	0.1	0.679741	0.703897
0	1	1.194617	1.224377
0	2	1.579317	1.615502
1	0.1	0.730548	0.754673
1	1	1.765922	1.793399
1	2	2.82033	2.850088

In recent years, there has been an increasing trend to emphasize the importance of the interfacial thermal resistance between nanoparticles and base fluids (see for example, Prasher et al. [47] and Jang and Choi, [48]). The thermal interfacial resistance (*Kapitza resistance*) is believed to exist in the adjacent layers of the two different materials; the thin barrier layer plays a key role in weakening the effective thermal conductivity of the nanoparticle.

Li [49] revisited the model of Koo and Kleinstreuer [50] and combined β and f functions to develop a new g'-function which captures the influences of particle diameter, temperature and volume fraction. The empirical g'-function depends on the type of nanofluid [50]. Also, by introducing a thermal interfacial resistance$R_{\mathrm{f}} = 4 \times 10^{-8}\mathrm{km}^2/\mathrm{W}$ the original k_p in Eq. (9) was replaced by a new $k_{\mathrm{p,\,eff}}$ in the form:

$$R_{\mathrm{f}} + \frac{d_{\mathrm{p}}}{k_{\mathrm{p}}} = \frac{d_{\mathrm{p}}}{k_{\mathrm{p,eff}}}\,. \tag{14}$$

Table 4 Effects of different kind of nanoparticles on Nusselt number when $\phi = 0.04$

γ	Re	Nanoparticles	
		CuO	Al_2O_3
0	0.1	1.846686	1.70097
0	1	4.324278	4.113995
0	2	5.996721	5.711652
1	0.1	2.676284	2.540234
1	1	15.23057	15.03967
1	2	28.85855	28.59338

For different base fluids and different nanoparticles, the function should be different. Only water-based nanofluids are considered in the current study. For Al_2O_3–water and CuO–water nanofluids, this function follows the format:

$$g'(T,\phi,d_p) = \left(a_1 + a_2 \ln(d_p) + a_3 \ln(\phi) + a_4 \ln(\phi)\ln(d_p) + a_5 \ln(d_p)^2\right)\ln(T) + \left(a_6 + a_7 \ln(d_p) + a_8 \ln(\phi) + a_9 \ln(\phi)\ln(d_p) + a_{10} \ln(d_p)^2\right) \quad (15)$$

where the coefficients a_i ($i = 0, 1, \ldots, 10$) are based on the type of nanoparticles and also with these coefficients, Al_2O_3–water and CuO–water nanofluids have an R^2 of 96 and 98 %, respectively [50] (Tables 1 and 2). Finally, the KKL (Koo–Kleinstreuer–Li) correlation is written as:

$$k_{\text{Brownian}} = 5 \times 10^4 \phi \rho_f c_{p,f} \sqrt{\frac{\kappa_b T}{\rho_p d_p}}\, g'(T,\phi,d_p). \quad (16)$$

Koo and Kleinstreuer [45] further investigated laminar nanofluid flow in micro heat-sinks using the effective nanofluid thermal conductivity model they had established (Koo and Kleistreuer [45]). For the *effective viscosity* due to micro mixing in suspensions, they proposed:

$$\mu_{\text{eff}} = \mu_{\text{static}} + \mu_{\text{Brownian}} = \mu_{\text{static}} + \frac{k_{\text{Brownian}}}{k_f} \times \frac{\mu_f}{\text{Pr}_f} \quad (17)$$

where $\mu_{\text{static}} = \frac{\mu_f}{(1-\phi)^{2.5}}$ is viscosity of the nanofluid, as given originally by Brinkman.

Following Wang [40] we take the similarity transformation:

$$\eta = (r/a)^2,\ u = -\text{ca}[f(\eta)/\sqrt{\eta}],$$
$$w = 2cf'(\eta)z,\ \theta(\eta) = (T - T_\infty)/(T_w - T_\infty), \quad (18)$$

where prime denotes differentiation with respect to η.

Substituting Eq. (18) into Eqs. (5) and (7), we get the following ordinary differential equations:

$$\text{Re}.A_1.(1-\phi)^{2.5}(f'^2 - ff'') = \eta f''' + f'', \quad (19)$$

$$\eta\theta'' + (1 + \text{Re Pr} f.A_2/A_3)\theta' = 0, \quad (20)$$

where $\text{Re} = \text{ca}^2/2\upsilon_f$ is the Reynolds number, $\upsilon_f = \mu_f/\rho_f$ the kinematic viscosity, $\text{Pr} = \mu_f(\rho C_p)_f/(\rho_f k_f)$ is the

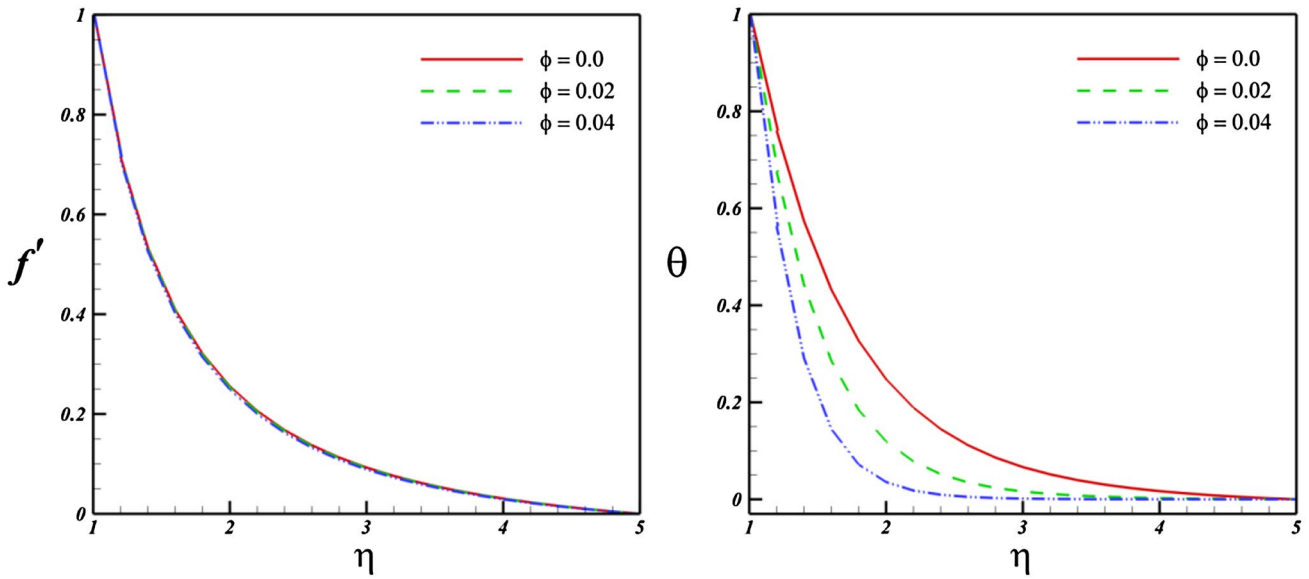

Fig. 3 Effect of nanoparticle volume fraction (ϕ) on velocity profile and temperature distribution when Re = 1, $\gamma = 1$ and Pr = 6.8(CuO–water)

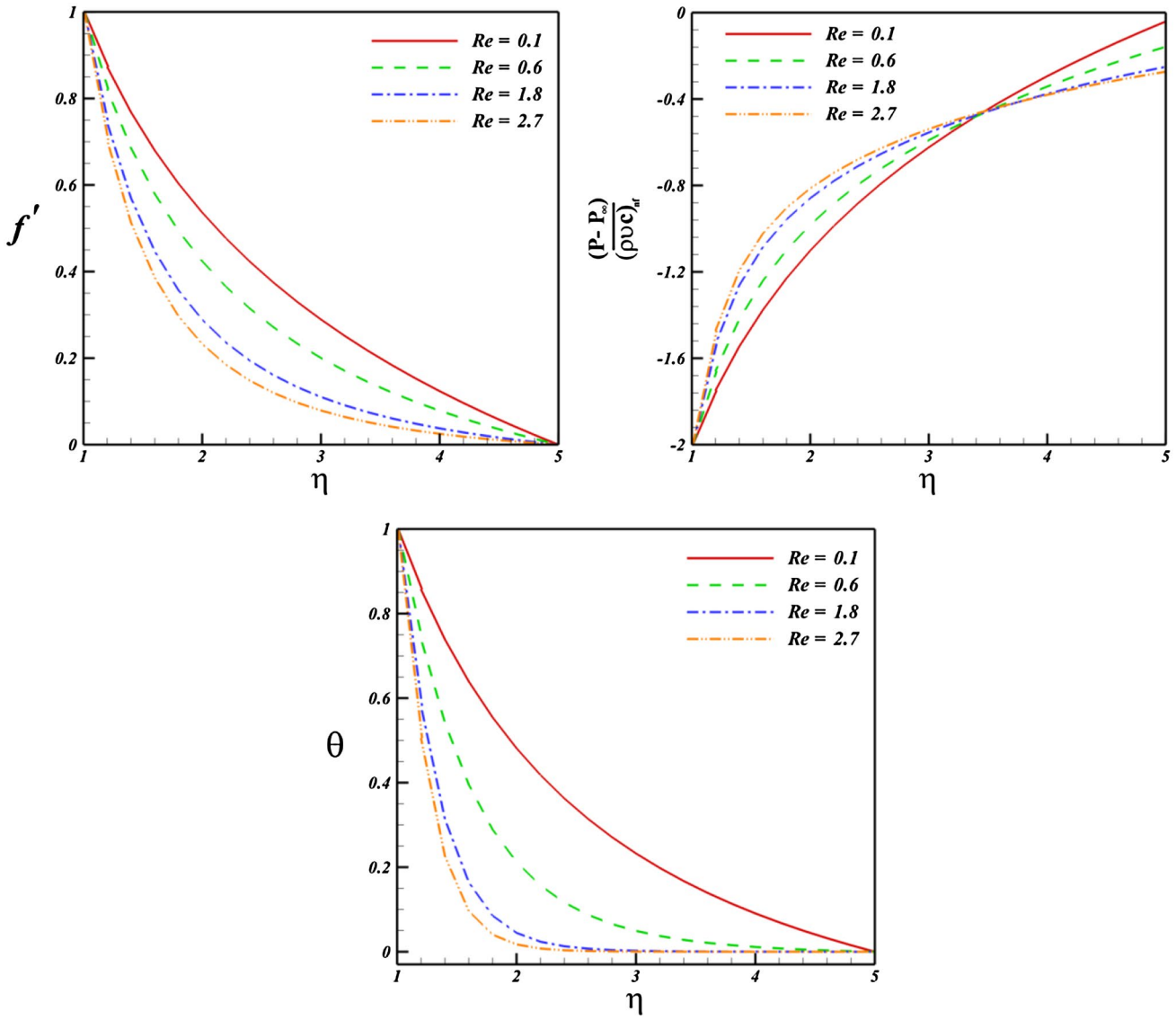

Fig. 4 Effect of Reynolds number on velocity profile, pressure distribution and temperature distribution when $\phi = 0.04$, $\gamma = 0$ and Pr = 6.8(CuO–water)

Prandtl number and A_1, A_2, A_3, A_4 are parameters having the following forms:

$$A_1 = (1-\phi) + \frac{\rho_s}{\rho_f}\phi \tag{21}$$

$$A_2 = (1-\phi) + \frac{(\rho C_p)_s}{(\rho C_p)_f}\phi \tag{22}$$

$$A_3 = \frac{k_{nf}}{k_f} = \frac{k_s + 2k_f - 2\phi(k_f - k_s)}{k_s + 2k_f + \phi(k_f - k_s)} \tag{23}$$

The boundary conditions (8) become

$$f(1) = \gamma, \quad f'(1) = 1, \quad \theta(1) = 1, \\ f'(\infty) \to 0, \quad \theta(\infty) \to 0. \tag{24}$$

The pressure (P) can now be determined from Eq. (6) in the form

$$\frac{P}{\rho_{nf}} = \frac{P_\infty}{\rho_{nf}} - \frac{c^2 a^2}{2\eta} f^2(\eta) - 2c\,\upsilon_{nf} f'(\eta), \tag{25}$$

i.e.,

$$\frac{P - P_\infty}{\rho_{nf} c\ \upsilon_{nf}} = -\frac{\mathrm{Re}}{\eta} A_1 .(1-\phi)^{2.5} f^2(\eta) - 2f'(\eta). \tag{26}$$

Physical quantities of interest are the skin friction coefficient (C_f) and the Nusselt number(Nu), which are defined as

$$C_f = \frac{\tau_w}{\rho w_w^2/2}, \quad Nu = \frac{a\, q_w}{k_f(T_w - T_\infty)}, \tag{27}$$

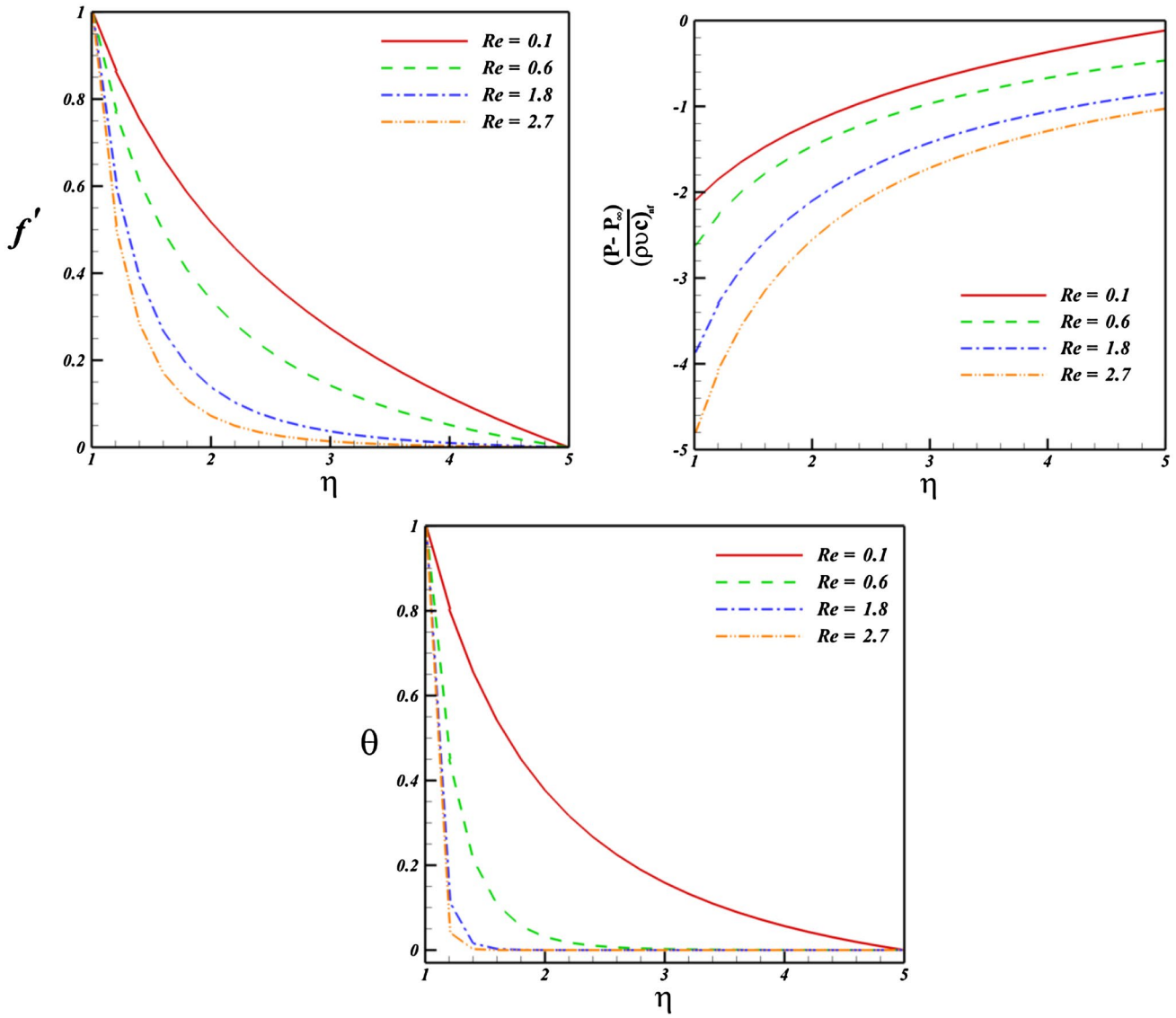

Fig. 5 Effect of Reynolds number on velocity profile, pressure distribution and temperature distribution when $\phi = 0.04$, $\gamma = 1$ and $\mathrm{Pr} = 6.8$ (CuO–water)

with k_f being the thermal conductivity of the base fluid. Further, τ_w and q_w are the surface shear stress and the surface heat flux, respectively, and they are given by

$$\tau_{\mathrm{w}} = \mu_{\mathrm{nf}}\left(\frac{\partial w}{\partial r}\right)_{r=a}, \quad q_{\mathrm{w}} = -k_{\mathrm{nf}}\left(\frac{\partial T}{\partial r}\right)_{r=a}, \tag{28}$$

i.e.,

$$\tau_{\mathrm{w}} = \frac{4\mu_{\mathrm{nf}}\, c\, z}{a} f''(1), \quad q_{\mathrm{w}} = -\frac{2k_{\mathrm{nf}}(T_{\mathrm{w}} - T_\infty)}{a}\theta'(1). \tag{29}$$

Using variables (27), we have:

$$C_{\mathrm{f}} \equiv \left|\frac{1}{A_1(1-\phi)^{2.5}} f''(1)\right|, \quad Nu \equiv -2\frac{k_{\mathrm{nf}}}{k_{\mathrm{f}}}\theta'(1). \tag{30}$$

3 Numerical method

Before employing the Runge–Kutta integration scheme, first we reduce the governing differential equations into a set of first-order ODEs.

Let $x_1 = \eta, x_2 = f, x_3 = f', x_4 = f'', x_5 = \theta, x_6 = \theta'$. We obtain the following system:

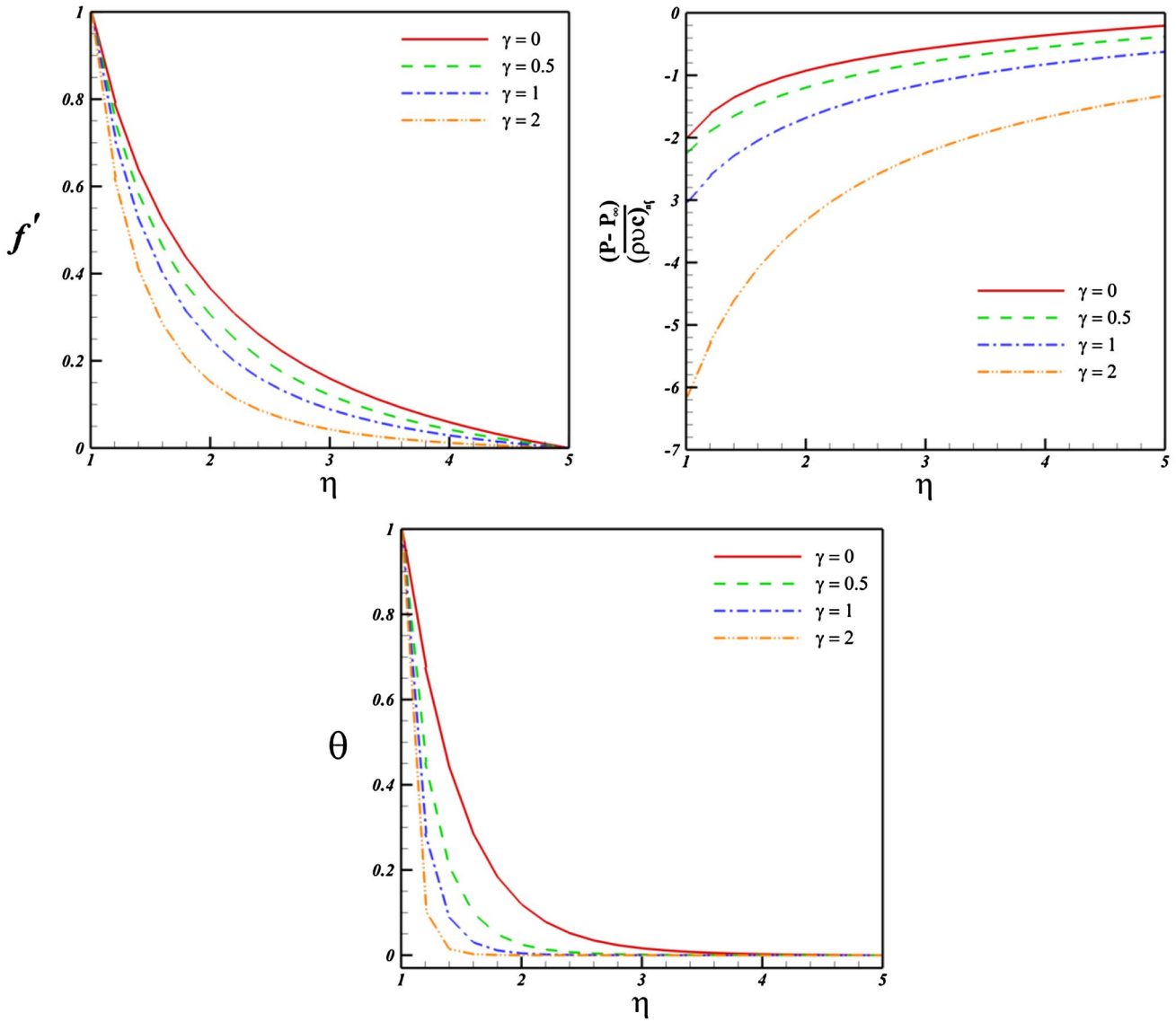

Fig. 6 Effect of suction parameter on velocity profile, pressure distribution and temperature distribution when $\phi = 0.04$, Re $= 1$ and Pr $= 6.8$ (CuO–water)

$$\begin{pmatrix} x_1' \\ x_2' \\ x_3' \\ x_4' \\ x_5' \\ x_6' \end{pmatrix} = \begin{pmatrix} 1 \\ x_3 \\ x_4 \\ \left[\mathrm{Re}.A_1.(1-\phi)^{2.5}(x_3^2 - x_4 x_2) - x_4\right]/\eta \\ x_6 \\ x_7 \\ -(1 + \mathrm{Re}\ \mathrm{Pr}\, x_2 A_2/A_3) x_7/\eta \end{pmatrix} \quad (31)$$

and the corresponding initial conditions are

$$\begin{pmatrix} x_1 \\ x_2 \\ x_3 \\ x_4 \\ x_5 \\ x_6 \end{pmatrix} = \begin{pmatrix} 1 \\ \gamma \\ 1 \\ u_1 \\ 1 \\ u_2 \end{pmatrix} \quad (32)$$

The above nonlinear coupled ODEs along with initial conditions are solved using fourth-order Runge–Kutta integration technique. Suitable values of the unknown initial conditions

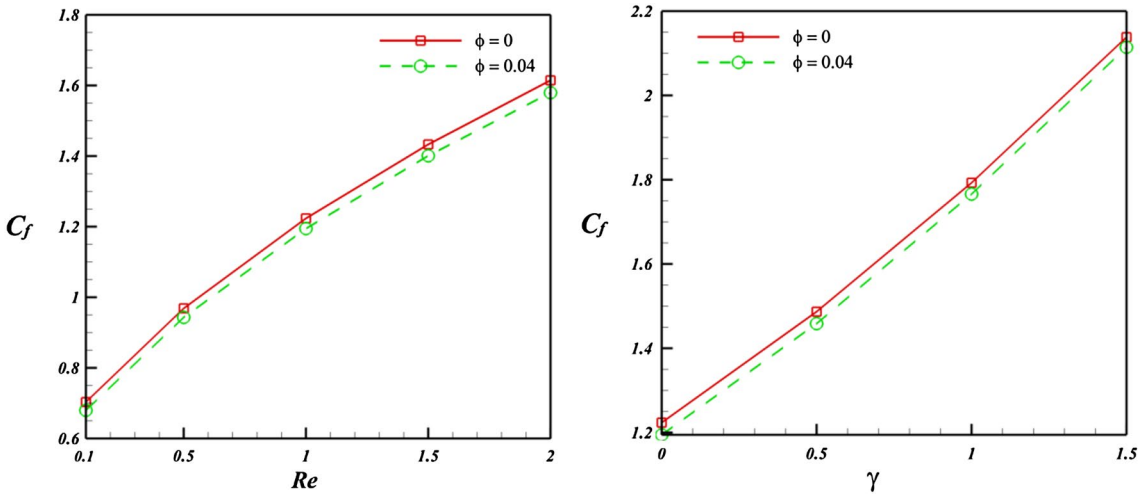

Fig. 7 Effects of the Reynolds number, suction parameter and nanoparticle volume fraction on skin friction coefficient when Pr = 6.8 (CuO–water)

u_1 and u_2 are approximated through Newton's method until the boundary conditions at $f'(\infty) \to 0, \quad \theta(\infty) \to 0$ are satisfied. The computations have been performed using MAPLE. The maximum value of$\eta = \infty$, to each group of parameters, is determined when the values of unknown boundary conditions at $x = 1$ do not change to a successful loop with error less than 10^{-6}.

4 Results and discussion

Nanofluid flow and heat transfer over a stretching porous cylinder are investigated. The governing equations and their boundary conditions are transformed to ordinary differential equations which are solved numerically using the fourth-order Runge–Kutta integration scheme featuring a shooting technique.

Effects of different types of nanofluid on velocity, temperature, skin friction coefficient and Nusselt number are shown in Fig. 2, Tables 3 and 4. It can be said that the shear stress and rate of heat transfer change with using different types of nanofluid. This means that type of nanofluid will be important in the cooling and heating processes. By selecting CuO as nanoparticle we can reach higher Nusselt number and smaller skin friction coefficient. So we use CuO–water to examine the effect of active parameters.

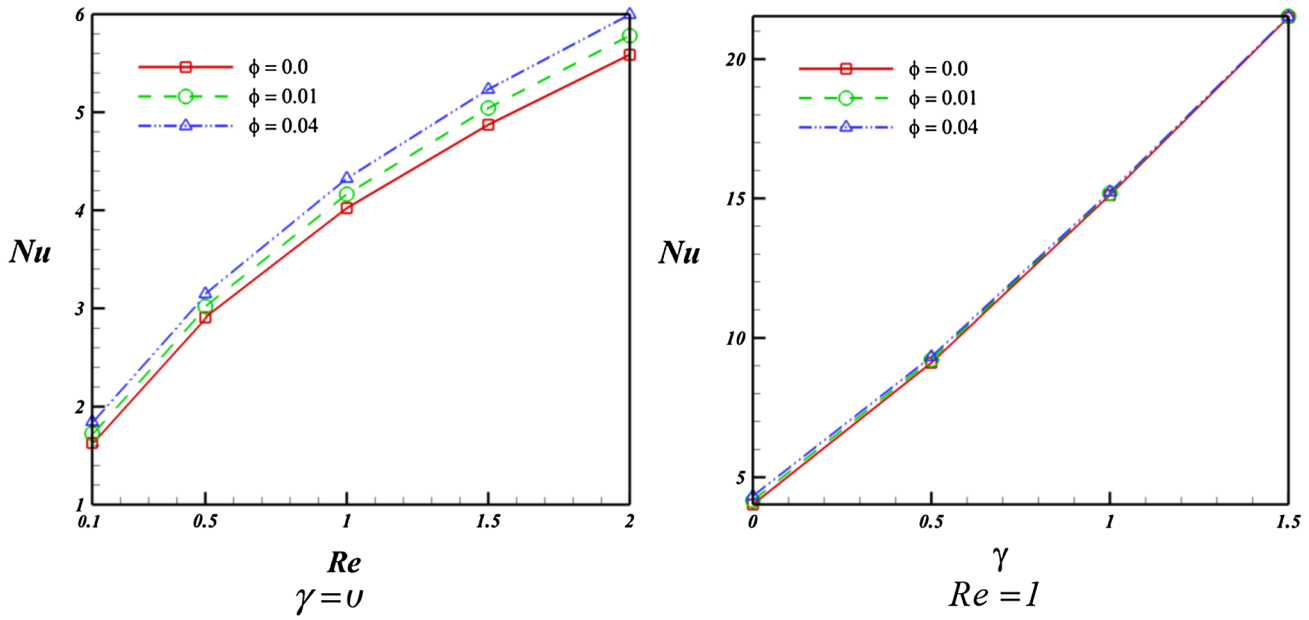

Fig. 8 Effects of the Reynolds number, suction parameter and nanoparticle volume fraction on Nusselt number when Pr = 6.8 (CuO–water)

Figure 3 shows the effect of nanoparticle volume fraction (ϕ) on velocity profile and temperature distribution. It has been found that when the volume fraction of the nanoparticle increases from 0 to 0.04, the thermal boundary layer thickness decreases while no sensible change occurs in velocity profile.

Effects of Reynolds number on velocity profile, pressure distribution and temperature distribution are shown in Figs. 4 and 5. As Reynolds number increases velocity and temperature profiles decrease. Pressure distribution increases with increase of Reynolds number near the cylinder while opposite trend is observed for further distance. When $\gamma = 1$, effects of Reynolds number on velocity profile and temperature distribution become greater while the effect of Reynolds number on pressure distribution has been changed. It means that as Reynolds number increases pressure decreases for all values of distant from the surface.

Figure 6 shows the effect of suction parameter on velocity profile, pressure distribution and temperature distribution. The velocity curves in this figure show that the velocity gradient at the surface increases as γ increases, which implies the increasing of the wall shear stress. The temperature is found to decrease as γ increases, also it decreases as the distance from the surface increases and finally vanishes in a large distance from the surface, which implies increasing in the wall temperature gradient and in turn increases the surface heat transfer rate. Hence, the Nusselt number increases as γ increases. Effect of suction parameter on pressure distribution is similar to that of Reynolds number in presence of suction.

Figure 7 shows the effects of the Reynolds number, suction parameter and nanoparticle volume fraction on skin friction coefficient. It can be found that skin friction coefficient decreases with increase of nanoparticle volume fraction while it increases with increase of Reynolds number and suction parameter.

Figure 8 depicts the effects of the Reynolds number, suction parameter and nanoparticle volume fraction on Nusselt number. Nusselt number is an increasing function of Reynolds number, suction parameter and nanoparticle volume fraction.

5 Conclusions

In the present study, two-dimensional nanofluid flow due to a stretching permeable tube has been investigated. The equations are solved numerically using the fourth-order Runge–Kutta method. Effects of nanoparticle volume fraction, types of nanofluid, suction parameter and Reynolds number on the flow and heat transfer characteristics have been examined. Results show that skin friction coefficient has direct relationship with Reynolds number and suction parameter but it has reverse relationship with nanoparticle volume fraction. It is observed that thermal boundary layer thickness decreases with increase of nanoparticle volume fraction, Reynolds number and suction parameter. The type of nanofluid is a key factor for heat transfer enhancement. The higher values of Nusselt number are obtained by selecting CuO nanoparticles.

References

1. Wang X-Q, Mujumdar AS (2007) Heat transfer characteristics of nanofluids: a review. Int J Therm Sci 46:1–19
2. Choi SUS (1995) Enhancing thermal conductivity of fluids with nanoparticles, The Proceedings of the 1995 ASME International Mechanical Engineering Congress and Exposition, San Francisco, USA, ASME, FED 231/MD 66 99–105
3. Das SK, Choi SUS, Yu W, Pradeep T (2007) Nanofluids: Sci Technol. Wiley, New Jersey
4. Sheikholeslami M, Gorji Bandpy M, Ellahi R, Zeeshan A (2014) Simulation of MHD CuO–water nanofluid flow and convective heat transfer considering Lorentz forces. J Magn Magn Mater 369:69–80
5. Rashidi MM, Abelman S, Freidooni Mehr N (2013) Entropy generation in steady MHD flow due to a rotating porous disk in a nanofluid, Intern J Heat Mass Transfer 62 515–525
6. Sheikholeslami M, Gorji-Bandpy M, Ganji DD (2014) MHD free convection in an eccentric semi-annulus filled with nanofluid. J Taiwan Inst Chem Eng 45:1204–1216
7. Hatami M, Sheikholeslami M, Hosseini M, Ganji DD (2014) Analytical investigation of MHD nanofluidflow in non-parallel walls. J Mol Liq 194:251–259
8. Sheikholeslami M, Gorji-Bandpy M, Ganji DD, Soleimani S (2014) Natural convection heat transfer in a nanofluid filled inclined L-shaped enclosure. IJST, Transac Mech Eng 38:217–226
9. Sheikholeslami M, Ganji DD (2014) Magnetohydrodynamic flow in a permeable channel filled with nanofluid, Scientia Iranica B 21(1), 203–212
10. Sheikholeslami M, Gorji-Bandpy M, Ganji DD, Rana P, Soleimani S (2014) Magnetohydrodynamic free convection of Al2O3-water nanofluid considering Thermophoresis and Brownian motion effects. Comput Fluids 94:147–160
11. Sheikholeslami Mohsen, Gorji-Bandpy Mofid (2014) Free convection of ferrofluid in a cavity heated from below in the presence of an external magnetic field. Powder Technol 256:490–498
12. Sheikholeslami M, Gorji-Bandpy M, Ganji DD, Soleimani S (2014) Thermal management for free convection of nanofluid using two phase model. J Mol Liq 194:179–187
13. Sheikholeslami M, Ganji DD (2014) Numerical investigation for two phase modeling of nanofluid in a rotating system with permeable sheet. J Mol Liq 194:13–19
14. Sheikholeslami M, Gorji-Bandpy M, Ganji DD (2014) Lattice Boltzmann method for MHD natural convection heat transfer using nanofluid. Powder Technol 254:82–93
15. Sheikholeslami M, Ganji DD (2014) Three dimensional heat and mass transfer in a rotating system using nanofluid. Powder Technol 253:789–796
16. Hatami M, Sheikholeslami M, Ganji DD (2014) Laminar flow and heat transfer of nanofluid between contracting and rotating disks by least square method. Powder Technol 253:769–779
17. Sheikholeslami M, Gorji-Bandpy M, Ganji DD, Soleimani S (2014) Heat flux boundary condition for nanofluid filled enclosure in presence of magnetic field. J Mol Liq 193:174–184

18. Sheikholeslami M, Hatami M, Ganji DD (2014) Nanofluid flow and heat transfer in a rotating system in the presence of a magnetic field. J Mol Liq 190:112–120
19. Sheikholeslami M, Ganji DD, Gorji-Bandpy M, Soleimani S (2014) Magnetic field effect on nanofluid flow and heat transfer using KKL model. J Taiwan Inst Chem Eng 45:795–807
20. Sheikholeslami M, Gorji-Bandpy M, Soleimani S (2013) Two phase simulation of nanofluid flow and heat transfer using heatline analysis. Intern Commun Heat Mass Transfer 47:73–81
21. Sheikholeslami M, Gorji-Bandpy M, Ganji DD (2013) Numerical investigation of MHD effects on Al2O3-water nanofluid flow and heat transfer in a semi-annulus enclosure using LBM. Energy 60:501–510
22. Sheikholeslami M, Gorji Bandpy M, Ellahi R, Hassan M, Soleimani S (2014) Effects of MHD on Cu-water nanofluid flow and heat transfer by means of CVFEM. J Magn Mag Mater 349:188–200
23. Sheikholeslami M, Bani Sheykholeslami F, Khoshhal S, Mola-Abasi H, Ganji DD, Rokni HB (2014) Effect of magnetic field on Cu–water nanofluid heat transfer using GMDH-type neural network, Neural Comput & Applic 25:171–178
24. Sheikholeslami M, Gorji-Bandpy M, Pop I, Soleimani S (2013) Numerical study of natural convection between a circular enclosure and a sinusoidal cylinder using control volume based finite element method. Intern J Thermal Sci 72:147–158
25. Ellahi R (2013) The effects of MHD and temperature dependent viscosity on the flow of non-Newtonian nanofluid in a pipe: analytical solutions. Appl Math Model 37(3):1451–1467
26. MM Rashidi, S Abelman, N Freidooni Mehr (2013) Entropy generation in steady MHD flow due to a rotating porous disk in a nanofluid, Intern J Heat Mass Transfer 62 515–525
27. Sheikholeslami M, Gorji-Bandpy M, Seyyedi SM, Ganji DD, Rokni HB, Soleimani S (2013) Application of LBM in simulation of natural convection in a nanofluid filled square cavity with curve boundaries. Powder Technol 247:87–94
28. Sheikholeslami M, Gorji-Bandpy M, Ganji DD (2013) Natural convection in a nanofluid filled concentric annulus between an outer square cylinder and an inner elliptic cylinder. Scientia Iranica, Transaction B: Mech Eng 20(4):1241–1253
29. Sheikholeslami M, Hatami M, Ganji DD (2013) Analytical investigation of MHD nanofluid flow in a semi-porous channel. Powder Technol 246:327–336
30. Sheikholeslami M, Gorji-Bandpy M, Ganji DD (2014) Natural convection heat transfer in a cavity with sinusoidal wall filled with CuO–water nanofluid in presence of magnetic field. J Taiwan Inst Chem Eng 45:40–49
31. Sheikholeslami M, Gorji-Bandpy M, Domairry G (2013) Free convection of nanofluid filled enclosure using lattice Boltzmann method (LBM). Appl Math Mech–Engl Ed 34(7):1–15
32. Sheikholeslami M, Gorji-Bandpy M, Ganji DD (2013) Soheil Soleimani, Effect of a magnetic field on natural convection in an inclined half-annulus enclosure filled with Cu–water nanofluid using CVFEM. Adv Powder Technol 24:980–991
33. Sheikholeslami M, Gorji-Bandpy M, Ganji DD, Soleimani S (2014) MHD natural convection in a nanofluid filled inclined enclosure with sinusoidal wall using CVFEM. Neural Compu Appl 24:873–882
34. Sheikholeslami M, Ganji DD (2013) Heat transfer of Cu-water nanofluid flow between parallel plates. Powder Technol 235:873–879
35. Soleimani S, Sheikholeslami M, Ganji DD, Gorji-Bandpay M (2012) Natural convection heat transfer in a nanofluid filled semi-annulus enclosure. Int Commun Heat Mass Transfer 39:565–574
36. Sheikholeslami M, Gorji-Bandpay M, Ganji DD (2012) Magnetic field effects on natural convection around a horizontal circular cylinder inside a square enclosure filled with nanofluid. Int Commun Heat Mass Transfer 39:978–986
37. Khan WA, Pop I (2010) Boundary-layer flow of a nanofluid past a stretching sheet. Int. J. Heat Mass Transfer 53:2477–2483
38. Hayat T, Abbas Z, Pop I, Asghar S (2010) Effects of radiation and magnetic field on the mixed convection stagnation-point flow over a vertical stretching sheet in a porous medium. Int J Heat Mass Transf 53:466–474
39. Hayat T, Qasim M (2010) Influence of thermal radiation and Joule heating on MHD flow of a Maxwell fluid in the presence of thermophoresis. Int J Heat Mass Transf 53:4780–4788
40. Wang CY (1988) Fluid flow due to a stretching cylinder. Phys Fluids 31:466–468
41. Al-Sanea SA (2004) Mixed convection heat transfer along a continuously moving heated vertical plate with suction or injection. Int J Heat Mass Transfer 47:1445–1465
42. Datta P, Anilkumar D, Roy S, Mahanti NC (2006) Effect of non-uniform slot injection (suction) on a forced flow over a slender cylinder. Int J Heat Mass Transfer 49:2366–2371
43. Kumari M, Nath G (2004) Mixed convection boundary layer flow over a thin vertical cylinder with localized injection/suction and cooling/heating. Int J Heat Mass Transfer 47:969–976
44. Ishak A, Nazar R, Pop I (2008) Uniform suction/blowing effect on flow and heat transfer due to a stretching cylinder. Appl Math Model 32:2059–2066
45. Koo J, Kleinstreuer C (2004) Viscous dissipation effects in micro tubes and micro channels. Int J Heat Mass Transf 47:3159–3169
46. Koo J (2004) Computational nanofluid flow and heat transfer analyses applied to microsystems, Ph.D Thesis, NC State University, Raleigh, NC
47. Prasher RS, Bhattacharya P, Phelan PE (2005) Thermal conductivity of nano scale colloidal solution. Phys Rev Lett 94:025901-1–025901-4
48. Jang SP, Choi SUS (2004) The role of Brownian motion in the enhanced thermal conductivity of nanofluids. Appl Phys Lett 84:4316–4318
49. Li J (2008) Computational analysis of nanofluid flow in micro channels with applications to micro-heat sinks and bio-MEMS, PhD Thesis NC State University, Raleigh, NC, the United States
50. Koo J, Kleinstreuer C (2005) Laminar nanofluid flow in micro-heat-sinks. Int J Heat Mass Transf 48:2652–2661